



PSR Report 1110

AD A 106751

THEORY OF ELECTRON-AVANCEMENT BREAKDOWN IN SOLIDS

- M. Sparks
- D. L. Mills
- R. Warren
- T. Holstein
- A. A. Maradudin
- L. J. Sham
- E. Loh, Jr.
- D. F. King



March 1981

Final Report
Contract F49620-79-C-0061

DTIC FILE COPY

Sponsored by
Air Force Office of Scientific Research
Bolling Air Force Base, D.C. 20332



PACIFIC-SIERRA RESEARCH CORP.

1456 Cloverfield Blvd. • Santa Monica, California 90404

81 11 06 03

Approved for public release

PSR Report 1110

(14) PSR-1110

(6)

THEORY OF ELECTRON-AVALANCHE BREAKDOWN IN SOLIDS

(10)

M/Sparks
D. L./Mills
R. Warren
T. Holstein
A. A./Maradudin
L. J. Sham
E. Loh, Jr.
D. F. King

(9) Final rpt.

(11)

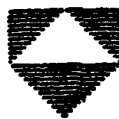
March 1981

(12) 7L

(15)

Final Report
Contract F49620-79-C-0061

Sponsored by
Air Force Office of Scientific Research
Bolling Air Force Base, D.C. 20332



PACIFIC-SIERRA RESEARCH CORP.

1425 Commercial Blvd. • Santa Monica, California 90404
AIR FORCE OFFICE OF SCIENTIFIC RESEARCH (AFSC)
NOTICE OF TRANSMITTAL TO DTIC
This technical report has been reviewed and is
approved for public release IAW AFR 190-12.
Distribution is unlimited.
MATTHEW J. KERPER
Chief, Technical Information Division

407486

PREFACE

This is the final report concluding Air Force Office of Scientific Research contract F49620-79-C-0061; it will be submitted to Physical Review for publication.

Accession For	
NTIS GRA&I	<input checked="" type="checkbox"/>
DTIC TAB	<input type="checkbox"/>
Unannounced	<input type="checkbox"/>
Justification	
By _____	
Distribution/ _____	
Availability Codes	
Avail and/or	
Dist	Special
A	

CONTENTS

PREFACE	ii
Section	
I. INTRODUCTION	2
II. AVERAGE-ELECTRON MODEL	8
III. DIFFUSION MODEL	12
IV. ELECTRON RELAXATION FREQUENCIES	17
V. NUMERICAL RESULTS	26
VI. INTERPRETATIONS AND CALCULATIONS USING SIMPLE MODELS ..	31
VII. ACKNOWLEDGMENTS	42
Appendix	
A. CALCULATION OF THE BREAKDOWN FIELD FOR CONSTANT D AND V	43
B. AN ANALYTIC EXPRESSION FOR THE MULTIPLICATION RATE β IN THE LIMIT OF A WEAK ELECTRIC FIELD	48
REFERENCES	52

Theory of electron-avalanche breakdown in solids

M. Sparks, D. L. Mills,* R. Warren, T. Holstein,*
A. A. Maradudin,* L. J. Sham,* E. Loh, Jr.,* D. F. King
Pacific-Sierra Research Corporation
Santa Monica, California 90404

↓
Electron-avalanche breakdown in solids is explained by a theory that is predictive and agrees with experimental results for the magnitude of the breakdown field and its temperature dependence, pulse-duration dependence, material-to-material variation, and wavelength dependence for $\lambda \gtrsim 1 \mu\text{m}$. The good agreement between experiment and theory with no parameters adjusted is obtained by using improved magnitudes and energy dependences of the electron-phonon relaxation frequencies. The contributions of both optical and acoustical phonons to electron loss and energy-space diffusion must be included. The breakdown field E_B is calculated by solving an eigenvalue equation obtained from the diffusion transport equation. Simple models and interpretations of the diffusion equation afford physical insight into breakdown and render the breakdown conditions predictable. Preliminary results indicate that the diffusion approximation fails for wavelengths considerably shorter than $1 \mu\text{m}$, where multiphoton absorption must also be considered.

delta
micron
 \gtrsim or $=$
micron
↑

I. INTRODUCTION

Damage of dielectric materials by high electric fields, which has been the subject of numerous experimental and theoretical investigations,^{1,2} has received renewed attention in recent years as a result of laser-damage experiments.^{2b} Electrical breakdown of dielectrics by lightning was one of the first known electrical phenomena; laboratory experiments on electrical breakdown in glass were initially conducted in 1799.¹ Despite many previous attempts¹⁻¹⁷ to develop a viable model of laser-induced damage to alkali halides, there has yet to appear a theory capable of simultaneously explaining the magnitude of the breakdown field as a function of temperature, wavelength, pulse duration, and variation from material to material.

Predictions of the electron-avalanche theory and a comparison of theoretical results with data available at the time were given by Sparks.¹⁷ A recent account of theoretical efforts by Soviet analysts was given by Gorshkov and coworkers,¹² and new data taken at the Lebedev Institute, along with further discussion of the theory, were presented by Manenkov.¹³ Difficulties with the electron-avalanche theory led Schmid and coworkers¹⁴ to explore such alternative mechanisms as multiphoton absorption combined with a possible rapid transfer of electron energy directly to the lattice by phonon emission--following a suggestion of Hellwarth¹⁵ that direct and rapid transfer of energy to the lattice, followed by its fracture, may account for the data. Preliminary results of the present investigation were summarized briefly elsewhere.¹⁸

The general features of the present theory, which mitigates the difficulties of the previous theories, are as follows: There must be a mechanism to generate a sufficient number of starting electrons to initiate the avalanche. These few starting electrons drift upward in energy in the conduction band through interaction with the laser field, retarded by energy loss to phonons. Each electron undergoes a random walk of progressively increasing kinetic energy until it attains a threshold energy ξ_1 . The electron then drops to the bottom of the conduction band. If an exciton has been created, its rapid photo-ionization injects a second electron into the bottom of the conduction band. The process is repeated until a sufficient electron density ($\sim 10^{18} \text{ cm}^{-3}$) has been created to damage the crystal, probably by excessive Joule heating.

This description of electron-avalanche breakdown is indeed also common to most previous theories. However, a cardinal reason for the good agreement of the present theory with experimental results, contrasted with the poor agreement of previous similar theories, is the use of more realistic electron-phonon scattering rates. Umklapp processes, which were neglected in previous treatments,^{16,17} are included in the electron-phonon relaxation frequencies. In other words, the phonons with which the electrons interact are not restricted to those in the first Brillouin zone, as in previous theories. Both acoustical and optical phonons are included in the interactions with electrons. Our theory retains the difference between the electron relaxation frequencies (or scattering rates) γ_k at which the electron loses its forward component of momentum and γ_L at which the electron loses

energy. The resulting magnitude and energy dependences of the electron-phonon scattering rates are essential differences between our model and those of previous investigations.

Another unique aspect of the present theory is the inclusion of the temperature dependence of the lattice constant and phonon frequencies. Without that dependence, the agreement with the measured temperature dependence of the breakdown irradiance--especially at $10.6 \mu\text{m}$ --is degraded. With the inclusion of the new electron scattering rates and the temperature dependence of the parameters, the common transport-equation approach can explain available data without introducing new mechanisms. In particular, the predictions of the theory agree well with the new Lebedev data.^{13,17}

The material-to-material variations of the breakdown electric field E_B in the present theory result from the values of the characteristic phonon frequency $k\omega_{ph}$, which is set equal to the Debye energy $k_B\theta_D$, and the electron-cation scattering cross section Q_a , which is scaled as the square of the ionic radius.

The electrons that are initially present or generated (those that start the avalanche) will be called the starting electrons. Most previous theories of electron-avalanche breakdown in solids at laser frequencies have either implicitly or explicitly assumed that starting electrons are present when the laser is turned on. Sparks¹⁷ showed that experimental data contradict that assumption. The starting electrons are not initially present; they must be generated--by an external source or by the laser field itself, for example. In microwave gas-breakdown experiments, it is well known that the starting electrons

must be generated. A radioactive source near the microwave cavity is commonly used to provide the starting electrons.

Since both processes--generation and acceleration--are required for breakdown, either the generation of the starting electrons or the avalanche process itself can determine the breakdown field. Processes by which the laser field can generate the starting electrons were discussed by Sparks.¹⁷ Only the avalanche process is considered here. The estimates of Sparks¹⁷ on electron generation--as well as the good agreement between experiment and the present theory, in which the breakdown is dominated by the avalanche process--partially justify not conducting a detailed investigation of starting-electron generation. In fact, the importance of generating the starting electrons will remain uncertain until verified experimentally.

If the electrical breakdown field E_B were dominated by starting electrons either initially present or generated, rather than by the avalanche process itself, the experimental value of E_B would generally be greater than that obtained when starting electrons are provided. If dominated by electrons initially present, E_B would vary from shot to shot, depending on the probability of a starting electron being present. Such variations are well known in microwave breakdown of gases, in which E_B can vary by well over an order of magnitude.

A major difficulty in obtaining agreement between theory and experiment is determining whether the experimental values of E_B are intrinsic. It is common practice to select only the greatest measured values of E_B . However, those retained still may not be the intrinsic values. Despite the inherent difficulty of determining

when an intrinsic value has been attained, it is likely that the Lebedev values at 1.06 and 10.6 μm are intrinsic because they agree so well with the present theory.

In using a differential form of the transport equation, we assume that the photon energy $h\nu$ is sufficiently small to be treated by differentials rather than differences. At high frequencies (wavelength $\lambda \lesssim 1 \mu\text{m}$, very roughly), the differential approximation gives rise to nonnegligible errors. This and other high-frequency effects will be considered in a subsequent publication.¹⁹

Sparks¹⁷ showed that the process in which an electron absorbs or emits both a photon and a phonon is sometimes important in electron-avalanche breakdown. This was called the Holstein process because Holstein²⁰ showed it to be the dominant mechanism determining the value of the conductivity in the limit $\omega\tau \gg 1$ --provided that $h\nu$ is sufficiently small to permit photon emission as well as absorption. The Holstein process is tacitly included here because the energy gain of the electron is treated in terms of the conductivity (which is controlled by the Holstein process in the limit $\omega\tau \gg 1$).

Table I lists processes not included in the present theory because they are believed to be negligible in careful experiments for $\lambda \geq 1.06 \mu\text{m}$, along with the expected effect on the value of E_B .

The major sections of this paper are as follows:

- I. Introduction
- II. Average-Electron Model
- III. Diffusion Model
- IV. Electron Relaxation Frequencies

- V. Numerical Results
- VI. Interpretations and Calculations Using Simple Models
- VII. Acknowledgments

II. AVERAGE-ELECTRON MODEL

In order to understand the diffusion model, which is the basis of the present investigation, first consider the average-electron model. Section I discussed the general features of most current models-- the acceleration of a conduction electron by the laser field, the loss of energy from the electron to the phonons, the generation of a second conduction electron accompanied by a loss of kinetic energy of the first electron, and the repetition of the process until the electron concentration is sufficient to damage the crystal.

In the average-electron model, which affords the simplest mathematical treatment of the general model, the average energy-loss rate to the lattice is $(d\mathcal{E}/dt)_L$ and the average energy-gain rate from the electric field is $(d\mathcal{E}/dt)_E$. Breakdown occurs when the gain exceeds the loss:

$$(d\mathcal{E}/dt)_E > (d\mathcal{E}/dt)_L \quad (2.1)$$

for all $\mathcal{E} < \mathcal{E}_I$, where \mathcal{E}_I is the energy at which the electron generates a second conduction electron by excitation across the electronic energy gap.

The rate at which the field \underline{E} adds energy to the electron is obtained from the wave-vector equation

$$\hbar(dk_z/dt + \gamma_k k_z) = eE_{pk} \exp(i\omega t), \quad (2.2)$$

where \underline{E} is along the z axis, k_z is the z component of the electron wave vector \underline{k} , $\gamma_k = 1/\tau_k$ is the transport (momentum loss) relaxation

frequency, and ω is the laser frequency. The steady-state solution is

$$k_z = \frac{e\tau_k}{\hbar(1 + i\omega\tau_k)} E_{pk} \exp(i\omega t) . \quad (2.3)$$

With current $\mathcal{J} = e\mathcal{v}$, where the z component v_z of the velocity \mathcal{v} is equal to $\hbar k_z/m^*$ and m^* is the electron effective mass, the rate at which the field puts energy into the electron is

$$(d\mathcal{E}/dt)_E = \frac{1}{2} \text{Re } \mathcal{J} \cdot \mathcal{E}^* = \frac{1}{2} \text{Re } \hbar e k_z E^*/m^* ,$$

where Re denotes the real part and \mathcal{E}^* is the complex conjugate of \mathcal{E} . Substituting Eq. (2.3) into this equation, using $E^2 \equiv \frac{1}{2} E_{pk}^2$ (where E is the root-mean-square value of the field), and taking the average over the electron distribution, we obtain

$$(d\mathcal{E}/dt)_E = \frac{1}{3} \sigma E^2 , \quad \sigma = \frac{e^2 \tau_k}{m^*(1 + \omega^2 \tau_k^2)} , \quad (2.4)$$

where σ is the electrical conductivity. Equation (2.4) is the well-known conductivity result for a single electron. Physically, the energy gain in Eq. (2.4) is small when the electron momentum is changed rapidly by interactions with the phonons. That is, in this dc limit of large γ_k (or, more precisely, small $\omega\tau_k$), the phonon collisions inhibit the acceleration of the electron by changing its momentum to the opposite direction from that imparted by the electric field.

In the opposite limit of slow momentum change, the energy gain in Eq. (2.4) is again small. For this case of $\omega\tau_k \gg 1$, the electron is first accelerated, then decelerated when the direction of the

electric field reverses. The process occurs many times before the electron undergoes a momentum-changing collision with a phonon. The energy gained during one half-cycle is lost during the following half-cycle. The maximum energy gain, which is a function of the momentum relaxation time τ_k , occurs at $\omega\tau_k = 1$; then, on the average, the electron direction is reversed every time the electric field reverses direction.

The rate at which the electron loses energy to the lattice is

$$(d\mathcal{E}/dt)_L = \hbar\omega_{ph}\gamma_L, \quad (2.5)$$

where ω_{ph} is the average phonon frequency and the energy-loss relaxation frequency γ_L is different from γ_k in Eq. (2.4), as discussed below. Equating Eqs. (2.4) and (2.5) gives the threshold value E_{V0} above which the electrons gain energy from the field

$$E_{V0} = \omega \left(\frac{3\hbar\omega_{ph}m^*}{e^2} \right)^{1/2} \left[\frac{\gamma_L}{\gamma_k} \left(1 + \frac{\gamma_k^2}{\omega^2} \right) \right]^{1/2}. \quad (2.6)$$

The resulting breakdown criterion that the electric field E must be greater than E_{V0} at all electron energies--that is,

$$E_B = E_{V0mx}, \quad (2.7)$$

where E_{V0mx} is the maximum value of E_{V0} , and E_B is the value of E at breakdown--is a fair zeroth-order approximation, provided the energy-dependent relaxation frequencies γ_L and γ_k are interpreted correctly. However, even with the proper interpretation of the relaxation frequencies, the average-electron result in Eqs. (2.6) and (2.7) is only

a rough approximation. As discussed below, the inadequacy of the average-electron result stems both from the difficulty of treating the energy dependence γ_L and γ_k properly, and from the neglect of electron diffusion in energy space. The problems are overcome by using the transport-equation approach discussed in the following section.

Before leaving the average-electron model, consider the multiplication rate β . As a result of the repeated doubling of the number of conduction electrons, their number N_e increases exponentially as $N_e = N_0 \exp(\beta t)$. The net energy gain, from Eqs. (2.4) and (2.5), is

$$d\mathcal{E}/dt = \frac{1}{3} \sigma E^2 - \hbar\omega_{ph} \gamma_L = \frac{1}{3} \sigma E_{V0}^2 \frac{E^2 - E_{V0}^2}{E_{V0}^2}. \quad (2.8)$$

Assuming that σ and E_{V0}^2 are independent of \mathcal{E} (that is, γ_k and γ_L independent of \mathcal{E}), integrating Eq. (2.8), and using the breakdown criterion of setting the pulse duration $t = t_p$ equal to $51/\beta$ as discussed in Sec. V, we obtain

$$\begin{aligned} \beta &= \frac{51 \hbar\omega_{ph} \gamma_L}{\mathcal{E}_I} \frac{E^2 - E_{V0}^2}{E_{V0}^2}, & \text{for } E > E_{V0}^2, \\ &= 0, & \text{for } E < E_{V0}^2. \end{aligned} \quad (2.9)$$

The value of β goes to zero at $E = E_{V0}$. For a high electric field $E^2 \gg E_{V0}^2$, Eq. (2.9) gives

$$\beta = 17 \mathcal{E}_I^{-1} \sigma E^2, \quad \text{for } E^2 \gg E_{V0}^2. \quad (2.10)$$

III. DIFFUSION MODEL

The central approach of the present investigation is to solve the appropriate transport equation by an eigenvalue method. The transport equation, detailed by Holway and Fradin,¹⁶ can be cast as a diffusion equation in energy space:

$$\partial n(\mathcal{E}, t)/\partial t + \partial J/\partial \mathcal{E} = 0, \quad (3.1)$$

where $n(\mathcal{E}, t)$ is the number of electrons with energy between \mathcal{E} and $\mathcal{E} + d\mathcal{E}$, and the energy-space current (the net number of electrons whose energy increases from a value less than \mathcal{E} to a value greater than \mathcal{E} per unit time) is

$$J(\mathcal{E}, t) = V(\mathcal{E})n(\mathcal{E}, t) - D(\mathcal{E})\partial n(\mathcal{E}, t)/\partial \mathcal{E}. \quad (3.2)$$

Here $V(\mathcal{E})$ and $D(\mathcal{E})$ are the effective velocity and diffusion coefficient in energy space, respectively. Both depend on energy, temperature, and laser frequency. For fields comparable to the breakdown field, ignoring small field-independent contributions to D , we obtain

$$V(\mathcal{E}) = \frac{1}{3} \sigma E^2 - \hbar \omega_{ph} \gamma_L, \quad D(\mathcal{E}) = \frac{2}{3} \mathcal{E} \sigma E^2, \quad (3.3)$$

where E is the root-mean-square electric field and σ is defined in Eq. (2.4). The boundary conditions are

$$n(\mathcal{E}_I, t) = 0, \quad (3.4)$$

corresponding to no electrons accelerated past the exciton threshold,
and

$$J(0, t) = 2J(\mathcal{E}_I, t) , \quad (3.5)$$

corresponding to the "flux doubling" feature of exciton creation followed by photoionization. Converting the transport equation to a diffusion equation [Eq. (3.1)] is extremely useful because well-known, intuitively understood diffusion results can be brought to bear on the electron-avalanche breakdown problem, as illustrated below.

The transport equation resulting in Eqs. (3.1) through (3.5) has been derived in detail by Holstein²⁰--starting with the Boltzmann equation, neglecting the spatial dependence of the electron distribution, and averaging over momentum directions to reduce the momentum dependence to an energy dependence. In starting with the Boltzmann differential equation, it is tacitly assumed that the photon energy $\hbar\omega$ and the phonon energies $\hbar\omega_q$ are sufficiently small that energy differences can be replaced by differentials. The transport-equation results in Eqs. (3.1) through (3.5) can also be obtained²¹ from a straightforward summation of transition probabilities.

The partial-differential equation (3.1) is converted to an ordinary-differential eigenvalue equation by using the approximation

$$n(\mathcal{E}, t) = n(\mathcal{E}) \exp(\beta t) . \quad (3.6)$$

Substituting Eq. (3.6) into Eq. (3.1) gives the eigenvalue equation

$$dJ(\mathcal{E})/d\mathcal{E} = \beta n(\mathcal{E}) . \quad (3.7)$$

The eigenvalue β is the multiplication rate, and the eigenfunction $n(\xi)$ is the electron density in energy space. When the laser is first turned on, the initial electron distribution $n(\xi, 0)$ is not of the form assumed in Eq. (3.6). However, the initial distribution quickly develops into the eigenfunction distribution $n(\xi)$ in a time of the order of the diffusion time constant

$$\tau_{\text{dif}} = \xi_1^2/D . \quad (3.8)$$

In fact, for the exactly solvable example of $V = 0$ and D constant, the approach time to $n(\xi)$ is a factor of ten shorter than τ_{dif} .²¹ Since τ_{dif} is in the subpicosecond region in cases considered to date, the form $n(\xi)$ is attained over essentially the full pulse duration, and the approximate eigenvalue solution is quite accurate.

The accuracy of the eigenvalue-equation solution has also been demonstrated explicitly by expanding a representative initial electron distribution $n(\xi, 0)$ in the eigenfunctions. Then the projection of $n(\xi, 0)$ on the eigenfunction with positive real β (as discussed below) grows according to Eq. (3.6) for all $t > 0$, and the projections on the other eigenvectors decay rapidly. Dual-space eigenfunctions must be used in the scalar products with which the expansion coefficients are computed, because the system operator is non-Hermitian.

An eigenvalue β with a positive real part corresponds to an electron concentration that increases exponentially in time [according to Eq. (3.6)], as expected for the avalanche process. The eigenvalue problem defined by the differential equation (3.7), with boundary conditions in Eqs. (3.4) and (3.5), is non-Hermitian and nonpositive

definite; thus there is no assurance that either real eigenvalues or positive eigenvalues exist, though the eigenvalues β must occur in complex-conjugate pairs. Insight is gained from three simple cases with exact solutions to the eigenvalue problem:

1. $V(\mathcal{E}) = -V_0 = \text{constant}$ and $D(\mathcal{E}) = D_0 = \text{constant}$.
2. $V(\mathcal{E}) = -V_0 = \text{constant}$, with $V_0 > 0$, and $D(\mathcal{E}) = D_1\mathcal{E}$.
3. $V(\mathcal{E}) = V_0 - V_1\mathcal{E}$ and $D(\mathcal{E}) = 2V_0\mathcal{E}$.

These cases are discussed elsewhere.²¹ In all three, there is one and only one eigenvalue with a positive real part (when E is sufficiently large), and the imaginary part of that eigenvalue is zero. All others have $\text{Re}(\beta) < 0$, which corresponds to an exponentially decreasing electron concentration. In our numerical work, we have always found one and only one eigenvalue on the positive real axis. We suspect that this is a general feature of the present problem, but we have no proof.

The boundary conditions in Eqs. (3.4) and (3.5) are unrealistic in one regard. After creation and subsequent photoionization of the exciton, both electrons cannot appear together at precisely zero energy, but are in fact injected into the band energy over an energy interval with finite width controlled by both the exciton linewidth (for sodium chloride at room temperature, a few tenths of a volt) and the energy dependence of the photoionization cross section. In our numerical work, we have explored the sensitivity of the solution to this boundary condition by modifying Eq. (3.6) with a source term that distributes a total of two electrons over a finite energy interval near the bottom of the conduction band, for each electron that strikes the threshold

for exciton creation at ξ_1 . The solution is affected only slightly by that procedure, even when the "injection width" is several tenths of an electron volt.

IV. ELECTRON RELAXATION FREQUENCIES

The transport relaxation frequency γ_k and the energy-loss parameter $\hbar\omega_{ph}\gamma_L$ are obtained from the expressions

$$\gamma_k = \sum_{\pm} \sum_{\underline{q}} \sum_{\underline{k}} (1 - \hat{k} \cdot \hat{k}') p_{q\pm}(\underline{k}, \underline{k}') \quad (4.1)$$

and

$$\hbar\omega_{ph}\gamma_L = N(\mathcal{E})^{-1} \sum_{\pm} \sum_{\underline{q}} \sum_{\underline{k}} \sum_{\underline{k}'} (\pm \hbar\omega_q) p_{q\pm}(\underline{k}, \underline{k}') \delta(\mathcal{E} - \mathcal{E}_{\underline{k}}), \quad (4.2)$$

where the caret ($\hat{\cdot}$) denotes a unit vector, $p_{q\pm}(\underline{k}, \underline{k}')$ is the probability that an electron is scattered from \underline{k} to \underline{k}' by absorption or emission (\pm) of a phonon of wave vector \underline{q} and frequency ω_q , δ is the Dirac δ function, and $N(\mathcal{E})$ is the density of states in the conduction band. The summations over \underline{q} include summations over phonon branches. The expression in Eq. (4.2) provides the value of the rate of energy loss $\hbar\omega_{ph}\gamma_L$ directly, rather than γ_L . A value for γ_L itself can be obtained by setting the average phonon energy $\hbar\omega_{ph}$ equal to the Debye energy

$$\hbar\omega_{ph} = k_B \theta_D, \quad (4.2a)$$

where θ_D is the Debye temperature and k_B is the Boltzmann constant.

First consider the contribution of the longitudinal-optical phonons to γ_k . In polar materials such as the alkali halides, the electrons couple strongly to long-wavelength longitudinal-optical phonons as a result of the macroscopic electric field they generate.

Within the framework of a model in which the electron moves in a parabolic band with effective mass m^* , it is straightforward to derive the contribution to γ_k from Fröhlich scattering,²² as the scattering from the longitudinal-optical phonons is called. When the electron energy \mathcal{E} is large compared with the longitudinal-optical phonon frequency $\hbar\omega_{LO}$, the result of evaluating the summations in Eq. (4.1) is¹⁷

$$\gamma_{kLO} = \frac{e^2 m^{*1/2} \omega_{LO}}{\sqrt{2} \hbar \mathcal{E}^{1/2}} \left(\frac{1}{\epsilon_\infty} - \frac{1}{\epsilon_0} \right) (1 + 2n_{LO}), \quad (4.3)$$

where $n_{LO} = [\exp(\hbar\omega_{LO}/k_B T) - 1]^{-1}$ is the number of thermal longitudinal-optical phonons present in thermal equilibrium at temperature T , and ϵ_0 and ϵ_∞ are the static and high-frequency dielectric constants, respectively.

The corresponding result for $\hbar\omega_{ph} \gamma_L$ from Fröhlich scattering is

$$\hbar\omega_{ph} \gamma_L = \frac{(2m^*)^{1/2} e^2 \omega_{LO}^2}{\mathcal{E}^{1/2}} \left(\frac{1}{\epsilon_\infty} - \frac{1}{\epsilon_0} \right) \ln \left(\frac{4\mathcal{E}}{\hbar\omega_{LO}} \right). \quad (4.4)$$

From the $\mathcal{E}^{-1/2}$ dependence displayed in Eqs. (4.3) and (4.4), we see that Fröhlich scattering is most important near the bottom of the conduction band. The $\mathcal{E}^{-1/2}$ behavior displayed in Eqs. (4.3) and (4.4) is valid only when $\mathcal{E} \gg \hbar\omega_{LO}$. The full, complex expression is approximated by rounding off the singularity by replacing \mathcal{E} with $2\hbar\omega_{LO}$ for electron energies $\mathcal{E} \leq 2\hbar\omega_{LO}$. This approximation has little influence on the results.

Next consider the contribution to γ_k from nonpolar phonons--that is, from acoustical and transverse-optical phonons. The probability

that an electron is scattered from \underline{k} to \underline{k}' by emission or absorption of a phonon of wave vector \underline{q} and frequency ω_q is given by

$$P_{q\pm}(\underline{k}, \underline{k}') = \frac{2\pi}{\hbar} |M_{kk'}|^2 \left(\frac{\hbar}{2MN\omega_q} \right) \Delta(\underline{k}' - \underline{k} \mp \underline{q}) \times (n_q + 1/2 \mp 1/2) \delta(\mathcal{E}_{k'} - \mathcal{E}_k \mp \hbar\omega_q), \quad (4.5)$$

where M is the effective ionic mass, N is the number of unit cells per unit volume, Δ is the Kronecker delta, δ is the Dirac δ function, and $M_{kk'}$ is the electron-phonon matrix element defined below. For acoustical phonons of long wavelength, M is the sum of the masses in the unit cell; for transverse-optical phonons of long wavelength, M is the reduced mass of the unit cell; and for zone boundary phonons, M is a weighted average of the mass on each sublattice. Since the extended zone scheme is used, \underline{q} is not restricted to the first Brillouin zone and the phonon frequency ω_q is a periodic function of the wave vector, with the periodicity of the Brillouin zone.

Within the framework of the simplest possible theory--the free-electron-diffraction theory with the Born approximation--the electron-phonon matrix element is²³

$$M_{kk'} = iV_a(\underline{k})(\underline{k} \cdot \hat{e}_q), \quad (4.6)$$

where $\underline{k} \equiv \underline{k} - \underline{k}'$, \hat{e}_q is the unit phonon eigenvector, and

$$V_a(\underline{k}) = n_a \int d\underline{r} \exp(-i\underline{k} \cdot \underline{r}) U_a(\underline{r}), \quad (4.7)$$

where n_a is the atomic density and $U_a(\underline{r})$ is the potential in a unit cell of the crystal. The validity of Eqs. (4.6) and (4.7) can be extended beyond the Born-approximation limit by eliminating $|v_a(\underline{k})|^2$ through use of the expression

$$\sigma_a(K) = \left(\frac{m^*}{2\pi\hbar n_a} \right)^2 |v_a(\underline{k})|^2 \quad (4.8)$$

for the cross section per unit solid angle $\sigma_a(K)$.

For sodium chloride, examination of the magnitude of the cross sections for scattering from Na^+ and Cl^- ions shows that, in the range of energies of interest here, the cross section for scattering from the large, polarizable chlorine is far greater than that of the sodium ion. The corresponding result is true for all alkali halides. Thus, $\sigma_a(K)$ is well approximated by the cross section for scattering by the negative ion. In the numerical calculations, the value of $\sigma_a(K)$ is taken as the free-ion cross section. In effect, that procedure extends the validity beyond the Born approximation because the full t-matrix treatment for scattering by the negative ion is used in the evaluation of $\sigma_a(K)$.

For values of q outside the Brillouin zone, the scattering events described by Eq. (4.5) are Umklapp processes. A proper description of Umklapp scattering requires a more detailed calculation of $M_{kk'}$. Even though the full t-matrix for scattering by the halide ion is used to evaluate $\sigma_a(K)$, the calculation in effect treats the electron wave function using a one-plane-wave approximation. This leads to a non-physical divergence in $p_{q\pm}(\underline{k}, \underline{k}')$ whenever the wave-vector transfer

equals a reciprocal lattice vector \underline{G} because--as \underline{q} approaches \underline{G} for the three acoustical branches of the phonon spectrum-- ω_q approaches zero while $M_{kk'}$ remains finite. A proper treatment of the electron-phonon matrix element,²⁴ which is equivalent to at least a two-plane-wave approximation of the matrix element, shows that the electron-phonon matrix element vanishes as \underline{k}' approaches $\underline{k} + \underline{G}$, and that the cross section varies smoothly near these special values of wave-vector transfer.

When \underline{q} lies outside the first Brillouin zone, the phonon frequencies are approximated with suitable weighted averages of zone-boundary phonon frequencies, and an average is taken over the directions of the phonon eigenvector \hat{e}_q . That approximation properly includes the effect of the factor $(\underline{k} \cdot \hat{e}_q)^2$ on the energy variation of the cross section as well as the correct volume of phase space available to the electron in its final state. The approximated value of the cross section then has the correct overall energy dependence, with a reliable semiquantitative estimate of its magnitude at large electron energies where Umklapp scattering dominates.

The limit of small electron wave vectors is $k \lesssim k_{BZ}/2$ and $\mathcal{E} \ll \mathcal{E}_{BZ}/2$, where k_{BZ} is the wave vector of an electron at the Brillouin zone boundary. If we use that limit in evaluating the summations in Eq. (4.1)--with only the summations over acoustical phonons included, because the available phase space with $q < 2k$ is small--we obtain

$$\gamma_k(\mathcal{E}) = \frac{Q(\mathcal{E})\mathcal{E}}{8a_0^3 M_{\Sigma} c_{\ell} k^5} \int_0^{2k} dq q^4 \coth \frac{\hbar c_{\ell} q}{2k_B T}, \quad \text{for } \mathcal{E} < \frac{1}{2} \mathcal{E}_{BZ}, \quad (4.9)$$

where a_0 is the lattice constant, M_Σ is the total mass of the unit cell, c_ℓ is the sound velocity, k is the wave vector of the electron, and $Q(\xi) \equiv 4\pi\sigma_a(\xi)$ is the total cross section integrated over all solid angles. In the limit of small k , Eq. (4.9) gives

$$\gamma_k(\xi) = \frac{1}{(2m^*)^{1/2}} \frac{k_B T}{a_0^3 M_\Sigma c_\ell^2} \xi^{1/2} Q(\xi) \quad (4.10)$$

for a parabolic band with effective mass m^* .

In the opposite limit $k \gg k_{BZ}/2$, the electron effective mass is approximated with the free-electron mass m_0 and the corresponding result is

$$\gamma_k(\xi) = \frac{2\pi^2 \xi^2 Q(\xi)}{a_0^6 M_{>} m_0} \left(\frac{\xi}{\xi_{BZ}} \right)^{3/2} \left[\frac{(1 + 2n_{LA})}{\omega_{LA}} + 2 \frac{(1 + 2n_{TA})}{\omega_{TA}} \right], \quad (4.11)$$

where ω_{LA} and ω_{TA} are the frequencies of longitudinal and transverse phonons at the Brillouin zone boundary, respectively, and the effective mass M is chosen as $M_{>}$ --the heaviest constituent mass in the unit cell.

In the numerical calculations, we use a straightforward extrapolation between the low-energy-dominated relaxation frequency in Eq. (4.9) and the high-energy, Umklapp-dominated relaxation frequency in Eq. (4.11). The high-energy behavior of $\gamma_k(\xi)$ displayed in Eq. (4.11) is a crucial feature of our analysis. Both Holway and Fradin¹⁶ and the Soviet analysts^{12,13} neglected Umklapp scattering, thereby missing the dominant contribution to the relaxation frequencies for electron energies high in the conduction band.

Holway and Fradin approximated the acoustical phonon scattering with an expression similar to Eq. (4.9), but replacing the upper limit on the integral with a constant for the case of $\mathcal{E} > \mathcal{E}_{BZ}/2$. Using that constant, high-energy upper limit is equivalent to including only normal processes in the expression for $\gamma_k(\mathcal{E})$. In that case, the scattering rate decreases with energy at high energies--in qualitative contrast to Eq. (4.11)

The Soviet work employed an expression equivalent to Eq. (4.10), but with Fröhlich scattering ignored. The resulting form for $\gamma_k(\mathcal{E})$ was extrapolated to energies beyond \mathcal{E}_{BZ} , thereby underestimating the strength of the acoustical phonon scattering at high energies.

Finally, consider the contribution to $f_{\omega_{ph}}\gamma_L$ from nonpolar scattering. In calculating that contribution, the phonon frequencies that appear in the Dirac δ function in Eq. (4.5) are neglected, and approximations similar to those above are used. For scattering from a single phonon branch, this yields

$$f_{\omega_{ph}}\gamma_L = \frac{n_a v(\mathcal{E}) \hbar^2}{2M} \int d\Omega(\hat{k}') \sigma_a(K) (\underline{K} \cdot \hat{e}_q)^2, \quad (4.12)$$

where $v(\mathcal{E})$ is the velocity of an electron of energy \mathcal{E} . In the low-energy limit, where only long-wavelength acoustical phonons contribute, evaluating the integral in Eq. (4.12) gives

$$f_{\omega_{ph}}\gamma_L = 2n_a v(\mathcal{E}) Q(\mathcal{E}) \frac{m^*}{M_\Sigma}. \quad (4.13)$$

For $\mathcal{E} > \mathcal{E}_{BZ}/2$, m^* is replaced with the free-electron mass m_0 and M_Σ is replaced with M_γ . The numerical calculation of the Fröhlich

contributions to γ_k and $1/\omega_{ph}\gamma_L$ is straightforward. Only the value of m^* near the bottom of the conduction band is needed. The usual approximation $m^* \approx m_0/2$ is used, where m_0 is the free-electron mass.

To calculate the nonpolar phonon contributions to γ_k and γ_L , the cross section $Q_a(\xi)$ for scattering of an electron by the halide ion is replaced with its value $Q_a(\xi_I)$ at the exciton energy. Then $Q_a(\xi_I)$ is estimated from molecular scattering data. For example, the cross section for electron scattering from the molecule HCl is dominated by scattering from the Cl^- ion. Thus, we approximate $Q_a(\xi_I)$ with the HCl cross section, which has the value $Q(\xi_I) \approx 0.35 \text{ nm}^2$ at 8 eV. For the other alkali halides, we use the scaling $Q(\xi_I) = (r_h/r_{NaCl})^2 0.35 \text{ nm}^2$, where r_h is the ionic radius of the halide ion. The estimated values of $Q(\xi_I)$ for sodium chloride and the other alkali halides are some of the major uncertainties in obtaining quantitative values for the acoustical phonon contributions to γ_k and γ_L . The phonon frequencies are approximated using $\omega_{TA} = c_T k_{BZ}$ and $\omega_{LA} = c_L k_{BZ}$, for $q \geq k_{BZ}$, where k_{BZ} is the diameter of a spherical Brillouin zone chosen to have volume equal to the real Brillouin zone.

The temperature dependence of the relaxation frequencies is determined both by the explicit temperature dependence of the Bose-Einstein phonon-occupation numbers and by the temperature dependence of the lattice constant and the phonon frequencies. Figures 1 and 2 show the magnitude and energy variations of γ_k and γ_L for sodium chloride at room temperature. The Fröhlich contribution and the acoustical phonon contribution are shown separately to illustrate their relative importance. The Fröhlich contribution is important only at

low energies, within one to two volts of the band edge. Figure 3 shows the full curves of γ_k and γ_L together.

Values of the parameters used in the numerical calculations are listed in Table II.

V. NUMERICAL RESULTS

The electron multiplication rate β was calculated--using Hamming's predictor-corrector method--by a careful numerical integration of the eigenvalue equation in Eq. (3.7), with boundary conditions defined by Eqs. (3.4) and (3.5). If we consider the behavior of β as a function of electric field and temperature, then the breakdown fields predicted by the model will be obtained from the $\beta(E)$ curves. The dependence of β on the electric field E is shown in Fig. 4 for sodium chloride at $1.06 \mu\text{m}$ and four temperatures. Similar curves for $10.6 \mu\text{m}$ are shown in Fig. 5. The dramatic increase in β with increasing E at low fields, $E^2 \ll E_{V0mx}^2$, is explained in Sec. VI and can be seen from the average-electron model, for which β goes exactly to zero, as in Eq. (2.9).

At high fields, $E^2 \gg E_{V0mx}^2$, the multiplication frequency has the general behavior

$$\beta \sim E^2, \quad \text{for } E^2 \gg E_{V0}^2, \quad (5.1)$$

as in Eq. (2.10) and as discussed in Sec. VI. The curves in Figs. 4 and 5 do not extend to sufficiently great electric fields to fully show the E^2 dependence, but we have verified that the quite general E^2 dependence is attained at high fields. The temperature variation of β displayed in Figs. 4 and 5 can be understood qualitatively, as also discussed in Sec. VI.

The breakdown field is easily obtained by calculating the multiplication frequency β as a function of electric field once a criterion

has been established for selecting the value of β . We use the criterion $\beta t_{\text{eff}} = 17$, where t_{eff} is the effective pulse duration. For Gaussian pulses, t_{eff} is set equal to one-third the total pulse duration because breakdown occurs principally near the center of the pulse. The strong variation of β with electric field ensures that breakdown occurs near the pulse center at the breakdown threshold.

In Fig. 6, the calculated temperature dependence of the breakdown field is shown for sodium chloride at 1.06 and 10.6 μm . The data reported by the Lebedev group are superimposed. At 1.06 μm , the agreement between measured and calculated values is excellent for variations in both magnitude and temperature of the breakdown field. At the lowest temperature, where the data fall well below our calculated values, the measured breakdown field may not be intrinsic.

At 10.6 μm , the calculated breakdown field is nearly independent of temperature, in accordance with the data. However, the calculated value of the breakdown field is smaller than the reported values by a factor of two. The smaller value of the theoretical threshold is in sharp, welcome contrast to previous theoretical results, which have been unable to explain the breakdown at the low experimental values of E_B . More complete information on the magnitude and energy variations of the acoustic phonon contribution to γ_k and γ_L --particularly their dependence on $Q(\mathcal{E}_1)$ --may remove that quantitative discrepancy. The value of the breakdown field at 1.06 μm is fairly insensitive to the value of $Q(\mathcal{E}_1)$ because E_B^2 is proportional to the ratio γ_L/γ_k , as discussed in Sec. VI. In contrast, agreement at 10.6 μm is improved markedly by an increased value of Q_a because E_B^2 is proportional to the product $\gamma_L\gamma_k$. Although it is feckless

to adjust the values of parameters to force theoretical results to fit experimental data, selecting the value of a single parameter can nevertheless improve the agreement between theory and experiment, as shown in Fig. 6, for which an adjusted value of Q_a was used, rather than the unadjusted value of $Q_a = 0.35 \text{ nm}^2$ (which is not accurately known).

The breakdown fields at $1.06 \mu\text{m}$ for several alkali halides are summarized in Fig. 7. The present theory provides an excellent account of the variation of the breakdown field from material to material.

In Fig. 8, the variation of the calculated breakdown field with pulse duration is compared with the experimental results of the Lebedev group;^{12,13} Fradin, Yablonovitch, and Bass;⁹ Smith, Bechtel, and Bloembergen;¹⁰ and Fradin, Bloembergen, and Letellier.²⁵ The theoretical values track the trends in the data nicely, though our calculated breakdown fields are somewhat larger than those measured by the Bloembergen group.

The theory adequately accounts for the data on magnitude, temperature dependence, pulse-duration dependence, frequency dependence, and material-to-material variation with no adjusted parameters. There are minor qualitative discrepancies at $10.6 \mu\text{m}$, which have at least four possible causes. First, even though the description of γ_k and $f_{\omega_{\text{ph}}} Y_L$ involves no adjustable parameters, the theory is in fact phenomenological. A more quantitative account of these basic relaxation rates may improve the agreement between theory and experiment. In particular, the calculated values are inherently less accurate at $10.6 \mu\text{m}$ than at $1.06 \mu\text{m}$ and other short wavelengths--because small-wave-vector phonons determine the breakdown at $1.06 \mu\text{m}$, whereas phonons with wave vectors $q \geq 2k_{\text{BZ}}$ determine the breakdown at $10.6 \mu\text{m}$.

Section VI shows that low-energy electrons determine the breakdown at $1.06 \mu\text{m}$, whereas high-energy electrons govern it at $10.6 \mu\text{m}$. The maximum phonon wave vector is $q = 2k$ (where $k \sim \mathcal{E}^{1/2}$ is the electron wave vector), as seen in the upper limit of the integral in Eq. (4.9). For phonon wave vectors q near $2k_{\text{BZ}}$, the results become more model-dependent. In the calculation of γ_L and γ_k in Sec. IV, special treatment is required to remove nonphysical divergences related to Q_a and factors of $1/\omega_q$, which diverges as ω_q approaches zero at $q = 2k_{\text{BZ}}$. A better treatment of the large-wave-vector phonon scattering should increase the theoretical values of E_B at $10.6 \mu\text{m}$.

Second, the inaccuracy of the value of $Q(\mathcal{E}_I)$ discussed above may account for the small discrepancies. Third, low theoretical $10.6 \mu\text{m}$ values of E_B may result from high experimental values due to spherical aberration,²⁶ as discussed in Sec. VI. Fourth, the breakdown at $10.6 \mu\text{m}$ may be limited by the generation of starting electrons, rather than by the avalanche process itself.

Other, less likely explanations include Raman scattering and diffusion of the electrons out of the focal volume (which is unlikely because the focal volumes at $10.6 \mu\text{m}$ are greater than those at $1.06 \mu\text{m}$ and because simple estimates indicate that real-space diffusion is negligible). Although certain low experimental values of E_B agree well with theory, those that are lower than the greatest reliable value are currently believed to be extrinsic. Finally, it is never certain that the measured breakdown field is the intrinsic value. However, in experiments where the intrinsic limit is not reached, the experimental values will usually be lower than the theoretical.

Thus, an extrinsic mechanism would not explain the high measured values of the Lebedev group.

VI. INTERPRETATIONS AND CALCULATIONS USING SIMPLE MODELS

Physical explanations of the results presented in Sec. V are informative, important, and invaluable in establishing intuition. The simplest model--the average-electron model discussed in Sec. II--affords a useful framework for discussion of the results, but by itself fails to account for experimental observations. Calculations based on the transport-equation approach discussed in Secs. III and IV agree well with experiment, but numerical solutions to differential equations without verification and interpretation are vacuous.

Constant-V and -D model. This model treats the transport equation in Sec. III exactly for the case in which V and D are constants, independent of energy. Proper application of the constant-V and -D model, for which Appendix A gives the exact solution of the diffusion equation, allows the calculation of E_B from simple closed-form expressions that require no numerical computation. The resulting accuracy of these highly simplified calculations is well within the range of accuracy of the model and values of the input parameters. Thus, the model results afford a simple method of obtaining values of E_B , as well as providing scalings and aiding intuition.

The closed-form results of the constant-V and -D model also illustrate the lowering of E_B below the average-electron value in Eq. (2.7), as well as other features of the general theory. Simple limiting forms of the breakdown field E_B and the multiplication rate β for the constant-V and -D model derived in Appendix A are

$$E_B = E_d E_{V0} , \quad (6.1)$$

where

$$E_d \cong [1 + b_i g + b_i (1 + b_i g)]^{-1/2} , \quad \text{for } E^2 \ll E_{V0}^2 , \quad (6.2a)$$

$$\cong (0.219 \xi_I / g \xi + 0.57)^{1/2} , \quad \text{for } E^2 \gg E_{V0}^2 , \quad (6.2b)$$

with

$$g \equiv f \omega_{ph} \gamma_L t_p / 51 \xi_I \quad (6.3)$$

and

$$\beta \cong (6 f \omega_{ph} \gamma_L \xi^2 / \xi_I^2 \sigma E^2) \exp(-E_{V0}^2 / E^2) , \quad \text{for } E^2 \ll E_{V0}^2 , \quad (6.4a)$$

$$\cong \frac{4.6 f \omega_{ph} \gamma_L \xi}{\xi_I^2 E_{V0}^2} (E^2 - 0.57 E_{V0}^2) , \quad \text{for } E^2 \gg E_{V0}^2 . \quad (6.4b)$$

Here E_{V0} defined in Eq. (2.6) is the value of E at which the energy-space velocity is equal to zero.

Calculation of E_B using the constant-V and -D model. In order to apply the constant-V and -D results to real problems--in which γ_k and γ_L are functions of energy, rather than constants-- $\gamma_k(\xi)$ and $\gamma_L(\xi)$ must be evaluated at appropriate values of ξ , and an effective value $\xi_{I\text{eff}}$ of ξ_I that is smaller than the real ξ_I must usually be chosen. The magnitude of the error in the resulting value of E_B depends on how well these values of γ_k , γ_L , and ξ_I (or, equivalently, E_{V0} , γ_L , and ξ_I) can be chosen. Fortunately, the shapes of the $\gamma_k(\xi)$ and $\gamma_L(\xi)$ curves are such that choice of the constants E_{V0} , γ_L , and ξ_I are obvious and

the accuracy of E_B is extremely good, as illustrated by the following examples.

In the discussion of V and D below, the quantity $E_{V0}^2 - E^2$ is a measure of the height of the barrier in energy space through which the electrons must diffuse. Thus, the high barrier extending from near-zero energy to $\mathcal{E} \cong 0.3\mathcal{E}_I$ for $1.06 \mu\text{m}$ in Fig. 9 virtually determines the value of E_B --because the value of $E_{V0}^2(\mathcal{E}) - E^2 \cong 500 (\text{MV/cm})^2$ at $\mathcal{E}/\mathcal{E}_I = 0.15$ is a factor of five greater than $\sim 100 (\text{MV/cm})^2$ at $\mathcal{E}/\mathcal{E}_I = 0.45$, and the value of E_B is sensitive to the barrier height. With $E_{V0} = 15.3 \text{ MV/cm}$, $\mathcal{E}_{I\text{eff}} = 0.2\mathcal{E}_I$, and $\gamma_L = 1.6 \times 10^{-14} \text{ s}^{-1}$ --all corresponding to the barrier shown as the dashed line in Fig. 9-- Eqs. (6.1), (6.2a), and (6.3) give $g = 460$, $E_d = 0.33$, and

$$\begin{aligned} E_B &= 5.1 \text{ MV/cm} , & \text{const. V and D, } 1.06 \mu\text{m} , \\ &= 5.6 \text{ MV/cm} , & \text{full diff. eq., } 1.06 \mu\text{m} . \end{aligned} \tag{6.5}$$

The approximate value of 5.1 MV/cm nearly matches the value of 5.6 MV/cm obtained from the numerical solution of the diffusion equation. The corresponding results for $10.6 \mu\text{m}$ for the narrow and wide barriers in Fig. 9 are, respectively, $g = 1.67 \times 10^5$ and 3.72×10^4 , $E_d = 0.25$ and 0.27 , and

$$\begin{aligned} E_B &= 0.72 \text{ MV/cm and } 0.70 \text{ MV/cm} , & \text{const. V and D, } 10.6 \mu\text{m} , \\ &= 0.68 \text{ MV/cm} , & \text{full diff. eq., } 10.6 \mu\text{m} , \end{aligned} \tag{6.5a}$$

again showing excellent agreement. The two barriers are two approximations to the actual curves. They are used to show the insensitivity of the results to the choice of the barrier in this case.

Magnitude of E_B . In the low-field limit $E^2 \ll E_{V0}^2$, which is valid for nanosecond pulses, the breakdown field in Eqs. (6.1) and (6.2a) is less than E_{V0} , a typical value being $E_B = 0.3E_{V0}$. Thus, the simple model illustrates the energy-space diffusion effect of reducing the value of E_B below E_{V0} for nanosecond pulses. That is, E_d in Eq. (6.1) is less than unity.

In the high-field limit $E^2 \gg E_{V0}^2$, which is approached for picosecond pulses, the breakdown field in Eqs. (6.1) and (6.2b) is greater than E_{V0} . The high-field limit is valid for sufficiently short pulse durations, because a decrease in the pulse duration requires an increase in the electric field in order for the electrons to be accelerated in the shorter time. Conversely, at shorter pulse durations such as nanoseconds, the electric field is small, and the inequality $E^2 \ll E_{V0}^2$ is satisfied.

The model shows that the average-electron value of E_B in Eq. (2.7) affords a very rough approximation to E_B . Moreover, the corrections from the transport-equation approach show E_B to be somewhat smaller than E_{V0} for nanosecond pulses and somewhat greater for picosecond pulses.

Frequency dependence of E_B . Sparks¹⁷ pointed out a quite general shortcoming of previous theories. The factor $(1 + \gamma_k^2/\omega^2)^{1/2}$ in Eq. (2.6) is commonly used because it comes from the conductivity in that equation. If τ_k were independent of frequency, as was well accepted at that time, the resulting theoretical frequency dependence of the breakdown electric field E_B would grossly disagree with experimental results. The resolution of that difficulty--and the reason for the

successful explanation of the frequency dependence of E_B by the present theory--is that τ_k in the simple average-electron model cannot be treated as a constant, independent of frequency. The value of $\tau_k(\omega)$ is of course independent of the laser frequency. However, as a result of the energy dependence of τ_k and τ_L , different effective values of τ_k must be used at different laser frequencies, as illustrated by the following example.

At 1.06 μm , the inequality $\gamma_k \ll \omega$ is valid; whereas at 10.6 μm , the inequality $\omega \ll \gamma_k$ is valid. Thus, Eq. (2.6) gives

$$E_{V0} \cong \omega(3f\omega_{ph}m/e^2)^{1/2}(\gamma_L/\gamma_k)^{1/2}, \quad \text{at } 1.06 \mu\text{m}, \quad (6.6)$$

and

$$E_{V0} \cong (3f\omega_{ph}m/e^2)(\gamma_L\gamma_k)^{1/2}, \quad \text{at } 10.6 \mu\text{m}. \quad (6.7)$$

Equation (6.6) shows that the 1.06 μm breakdown field is controlled by the ratio γ_L/γ_k , which is greatest at low electron energies, as illustrated in Fig. 1. The energy dependence of E_{V0} , which is proportional to $(\gamma_L/\gamma_k)^{1/2}$ at 1.06 μm , is plotted in Fig. 9. As mentioned above, $E_{V0}^2(\mathcal{E}) - E^2$ is a measure of the height of the barrier through which the electrons must diffuse. The obstacle to accelerating the electrons to energy \mathcal{E}_I occurs at low energy, where E_{V0} has the greatest value for the 1.06 μm laser frequency, as shown by Fig. 9. In contrast, at 10.6 μm , E_B is controlled by the product $\gamma_L\gamma_k$, which is greatest at high electron energies $\mathcal{E} \cong \mathcal{E}_I$, as shown by Figs. 1 and 9. Thus, the obstacle occurs at high energies $\mathcal{E} \cong \mathcal{E}_I$ for the 10.6 μm laser frequency.

Since low-energy electrons are important for inducing breakdown at 1.06 μm and high-energy electrons at 10.6 μm , the corresponding values of γ_k should be used in evaluating E_{V0} in Eq. (2.6). The small, low-energy value of γ_k from Fig. 1 should be used at 1.06 μm ; but the large, high-energy value of γ_k at 10.6 μm . (The corresponding values of γ_L must also be used, of course--but γ_L does not vary as strongly with energy as does γ_k .) The diffusion equation automatically accounts for the correct τ_k at all frequencies; only when considering the average-electron model must the appropriate τ_k be selected explicitly.

For wavelengths shorter than approximately one micrometer, $\omega\tau_k \gg 1$ is sufficiently well satisfied at all \mathcal{E} for the shape of the $E_{V0}(\mathcal{E})$ curves to be independent of ω --that is, $E_{V0}(\mathcal{E}) \sim \omega$. Thus, for $\lambda \lesssim 1 \mu\text{m}$, the diffusion transport theory gives $E_B \sim \omega$. However, any of several effects is expected to cause E_B to be lower than the diffusion-theory value at short wavelengths. These effects include the breakdown of the validity of replacing differences by differentials, the specific large-quantum processes discussed by Sparks,¹⁷ and multi-photon absorption.

Dependence of E_B on t_p , \mathcal{E}_I , $i\omega_{ph}\gamma_L$, and ω . In the low-field limit $E^2 \ll E_{V0}^2$, which is valid for nanosecond pulses, Eqs. (6.1) and (6.2a) show that E_B is weakly dependent on the parameters t_p and \mathcal{E}_I that appear in E_d , and is more strongly dependent on the parameters $i\omega_{ph}\gamma_L$ and ω that appear in E_{V0} . The weak dependence of the breakdown field on the bandgap (or, to be precise, on \mathcal{E}_I) and on the laser-pulse duration t_p for nanosecond pulses was at first surprising. However, the previously used, average-electron criterion for breakdown, $E_B = E_{V0}$, also gave E_B

independent of ζ_I and t_p . Furthermore, agreement with experimental data is good. In the high-field limit $E^2 \gg E_{V0}^2$, which is approached for picosecond pulses, Eqs. (6.1) and (6.2b) show E_B to be rather strongly dependent on all parameters-- t_p , ζ_I , $1/\omega_{ph} \gamma_L$, and ω .

Focal-volume dependence of E_B . In laser breakdown of gases, the diffusion of the electrons out of the focal volume (not to be confused with energy-space diffusion) is an important effect that determines the value of E_B . However, simple estimates indicate that the diffusion of electrons out of the focal volume in solids is negligible in all experiments reported to date. Another factor--the probability of having or generating a starting electron in the focal volume--could conceivably cause E_B to depend on the focal volume, as discussed in Sec. I.

Soileau and coworkers²⁶ suggested that spot-size scaling could possibly reconcile the results of various analysts. They proposed that the value of E_B should be a function of the focal-volume size because the probability of having a starting electron present decreases with volume. Verification of the spot-size scaling law--through, for example, experiments with starting electrons supplied by a separate source, or examination of the probabilistic nature of breakdown in small focal volumes and its deterministic nature in large focal volumes--is needed because the starting electrons are currently thought to be easily generated by lattice imperfections such as impurities, dislocations, or grain boundaries. Breakdown is thought to be controlled by the avalanche process rather than the generation of seed electrons. However, these hypotheses have not yet been supported either by experiment or convincing theory, so verification of the suggested mechanism giving the spot-size scaling would be useful.

Aaron, Ireland, and Grey Morgan²⁷ showed that "entirely spurious 'focal-length' dependence of I_{th} , which is not infrequently found in published literature" can result from irradiance reduction caused by spherical aberration. Extreme care in measurement is required to avoid the spurious focal-volume effects.

Shape of the $\beta(E)$ curves. The central features of the electric-field dependence of β illustrated by Figs. 4 and 5 result from quite general considerations that are independent of specific models. At high fields, the diffusion in energy space becomes negligible, and the electrons stream freely to the multiplication energy ξ_I according to the relation $d\xi/dt \cong (d\xi/dt)_E \sim \sigma E^2$. As discussed in Sec. II, that streaming gives $\beta \sim E^2$ at high fields. The E^2 dependence of β at high fields is also explicitly illustrated by the constant-V and -D result in Eq. (6.5).

At low fields, β decreases rapidly with decreasing E because the barrier height $E_{V0}^2(\xi) - E^2$ through which the electrons must diffuse becomes high. Indeed, in the average-electron model of Sec. II, β goes to zero at $E = E_{V0}$. For the diffusion model, β goes to zero rapidly as $\beta \sim \exp(-E_c^2/E^2)$, as shown quite generally in Appendix B. The explicit result in Eq. (6.4a) illustrates that general high-field result, with the characteristic electric field E_c equal to E_{V0} .

Temperature dependence of the $\beta(E)$ curves. In the important range of electron energies discussed below, the inequality $\omega \gg \gamma_k(\xi)$ is satisfied at 1.06 μm . At high temperatures, $\gamma_k(\xi) \sim T$ and $\hbar\omega_{ph}\gamma_L \sim T^0$ if the thermal expansion corrections are ignored. The electron gains energy from the electric field at the rate $2e^2\gamma_k E^2/m^*\omega^2$, according to

Eq. (2.4); thus, as the temperature increases, the electron is accelerated more efficiently by the field because γ_k increases. Since the loss $1/\omega_{ph}\gamma_L$ is nominally temperature-independent, β increases with temperature for fixed electric fields. Consequently, the electric field required for breakdown decreases as the temperature is raised, in agreement with the data.

Figure 4 shows the variation of β with temperature and wavelength at 10.6 μm . The variation of β with electric field at fixed temperatures is qualitatively similar to the 1.06 μm behavior, as expected, but its variation with temperature is more complex. As the temperature increases from 77 K to room temperature, β increases much as it does at 1.06 μm . Over most of that range, $\omega > \gamma_k(\mathcal{E})$ is satisfied for the important range of energies, and the behavior of β with temperature may be understood by the arguments of the previous paragraph. At room temperature and above, the inequality $\omega < \gamma_k(\mathcal{E})$ is satisfied; the electron thus gains energy from the electric field at the rate $2e^2E^2/3m^*\gamma_k$, according to Eq. (2.4). As the temperature increases, with γ_k nominally proportional to temperature, the electron is accelerated less efficiently, and β decreases with increasing temperature, in contrast to its behavior at 1.06 μm . Thus, β first increases with temperature, reaches a maximum, and then falls. Since the criterion for breakdown outlined below places the breakdown field near the maximum at room temperature, the breakdown field is fairly independent of temperature, again in accordance with the data.

Energy-space velocity and diffusion. The energy-space velocity V , which appears in Eq. (3.2) and is defined for the general case in

Eq. (3.3), determines the rate at which the electrons drift to higher energies for positive V , or to lower energies for negative V , as a result of the combined effects of E acceleration and γ_L loss. The energy-space diffusion coefficient D , which appears in Eq. (3.2) and is defined in Eq. (3.3), determines the rate at which electrons diffuse from energy-space regions of high electron concentrations to neighboring low-concentration regions.

The average-electron model of Sec. II is equivalent to neglecting the energy-space diffusion. In extending the average-electron model to include energy-space diffusion, the quantity $E_{V0}^2(\mathcal{E}) - E^2$ --when positive--is a measure of the height of the barrier through which electrons must diffuse to reach the multiplication energy \mathcal{E}_I . When $E_{V0}^2(\mathcal{E}) - E^2$ is negative, the electrons drift to higher energies even in the absence of diffusion. Neglecting diffusion yields $E_{V0}^2(\mathcal{E}) - E^2 \leq 0$ as the criterion for breakdown, as indicated in Eq. (2.7).

The value of $E_{V0}^2(\mathcal{E}) - E^2$ at which breakdown occurs is positive over at least part of the energy range $0 \leq \mathcal{E} \leq \mathcal{E}_I$ --which indicates that electron diffusion in energy space effectively increases the electron energy to \mathcal{E}_I . The electric field thus need not be as large as the value in Eq. (2.7) predicted by the average-electron theory. That discrepancy is one reason previous average-electron theories predicted values of E_B greater than measured values.

Physically, the lowering of E_B by diffusion occurs as follows: The process by which the electron energy is increased to the multiplication value \mathcal{E}_I involves many collisions of the electron with phonons. Some collisions (γ_L) cause the electron to lose energy, and some (γ_k) to gain energy from the electric field.

The average effect of the collisions determines the energy-space velocity. The deviations from the average determine the energy-space diffusion coefficient. For example, an electron that meets with fewer than the average number of energy-loss collisions, together with an optimum distribution of momentum-reversing collisions--gains energy faster than does an average electron. At dc, the optimum distribution of momentum-reversing collisions is none at all; electrons undergoing no collisions are continuously accelerated by the electric field. For $\omega \neq 0$, the optimum distribution is a reversal of the electron momentum every cycle of the electric field (at the null in E). Electrons so accelerated faster than average have been called lucky electrons.^{3,4,5} The diffusion equation accounts for lucky electrons automatically, of course.

VII. ACKNOWLEDGMENTS

This investigation was supported by the Air Force Office of Scientific Research.

Appendix A

CALCULATION OF THE BREAKDOWN FIELD FOR CONSTANT D AND V

Here we solve the eigenvalue equation obtained from the diffusion equation exactly for the case of constant diffusion coefficient D and velocity V . The solution for this simple model affords approximate values of the breakdown field E_B and the electron multiplication rate β in key limiting cases, and determines their dependence on the variables. The accuracy of these highly simplified calculations is consistent with that of the overall model.

For constant D and V , Eq. (3.2) becomes

$$J(\xi, t) = Vn(\xi, t) - D \partial n(\xi t) / \partial \xi . \quad (A.1)$$

Substituting into Eq. (3.1), the diffusion equation in energy space becomes

$$\partial n / \partial t = D \partial^2 n / \partial \xi^2 - V \partial n / \partial \xi . \quad (A.2)$$

Setting $\partial n / \partial t = \beta n$ under the approximation of Eq. (3.6) yields the eigenvalue equation

$$D d^2 n / d \xi^2 - V dn / d \xi - \beta n = 0 . \quad (A.3)$$

Equation (A.3) is cast into dimensionless form

$$d^2 n_d / d \xi_d^2 + U_d dn_d / d \xi_d - \beta_d n_d = 0 \quad (A.4)$$

by dividing t by $\tau_{dif} = \xi_1^2 / D$ and ξ by ξ_1 and introducing the dimensionless variables

$$n_d = n \xi_I, \quad \xi_d = \xi / \xi_I, \quad \beta_d = \beta \tau_{dif} = (g E_d)^{-1}, \quad (A.5a)$$

$$E_d = E / E_{V0}, \quad U_d = -V \tau_{dif} / \xi_I (1 - E_d^2) / E_d^2, \quad (A.5b)$$

$$g = (\hbar \omega_{ph} \gamma_L t_p / 51 \xi_I). \quad (A.5c)$$

Substituting the trial solution $n_d = \exp(\alpha \xi_d)$ into Eq. (A.4) and solving for α yields

$$\alpha_{\pm} = \frac{1}{2} U_d \pm r, \quad \text{where } r \equiv \left(\frac{1}{4} U_d^2 + \beta_d \right)^{1/2}. \quad (A.6)$$

The boundary conditions for the case of constant D and V are

$$n(\xi_I) = 0, \quad (A.7)$$

$$-D \, dn(0)/d\xi + Vn(0) = -2D \, dn(\xi_I)/d\xi,$$

or, in dimensionless form,

$$n_d(1) = 0, \quad (A.7a)$$

$$-dn_d(0)/d\xi_d - U_d n_d(0) = -2 \, dn_d(1)/d\xi_d.$$

The general solution to Eq. (A.4) that satisfies Eq. (A.7a) is

$$n_d = \exp[\alpha_+(\xi_d - 1)] - \exp[\alpha_-(\xi_d - 1)]. \quad (A.8)$$

Substituting Eq. (A.8) into Eq. (A.7a) and rearranging terms yields the transcendental equation for β

$$2e^{-U_d/2} = \cosh r - (U_d/2r) \sinh r, \quad (A.9)$$

which reduces to

$$\cosh [(B/D)^{1/2} \epsilon_1] = 2, \quad \text{for } V = 0. \quad (\text{A.10})$$

In the limit $1 \ll \exp \frac{1}{2} U_d$, writing $\cosh r$ and $\sinh r$ as $\frac{1}{2} [\exp(r) \pm \exp(-r)]$, with $U_d/2r \approx 1 - 2\beta_d/U_d^2$ in Eq. (A.9), we obtain the limiting cases of

$$\beta_d = U_d^2 e^{-U_d}, \quad \text{for } 1 \ll \exp \frac{1}{2} U_d, \quad (\text{A.11a})$$

$$\approx E_d^{-4} e^{-1/E_d^2}, \quad \text{for } E_d^2 \ll 1. \quad (\text{A.11b})$$

Substituting $U_d = (1 - E_d^2)/E_d^2$ and $\beta_d = (gE_d^2)^{-1}$ into Eq. (A.11a) and formally solving for E_d yields

$$E_d = \left\{ 1 + \ln g + \ln \left[(1 - E_d^2)^2 / E_d^2 \right] \right\}^{-1/2}$$

$$\approx [1 + \ln g + \ln(1 + \ln g)]^{-1/2}, \quad g \gg 1, \quad (\text{A.12})$$

or $E^2 \ll E_{V0}^2$. The breakdown field E_B can then be obtained using $E_B = E_d E_{V0}$.

The value of β in this small-field limit is obtained from Eq. (A.11b) by using the definitions of β_d and E_d in Eq. (A.5), with $E_{V0} = (3f\omega_{ph}\gamma_L/\sigma)^{1/2}$. This gives the result of Eq. (6.4a):

$$\beta \approx (6f\omega_{ph}\gamma_L \epsilon^2 / \epsilon_1^2 \sigma E^2) \exp(-E_{V0}^2/E^2), \quad \text{for } E^2 \ll E_{V0}^2.$$

In the other limit of high fields, $E_d^2 \gg 1$ ($E^2 \gg E_{V0}^2$), Eq. (A.5b) gives $U_d \cong -1$. By substituting $U_d = -1$ into Eq. (A.9) and expanding $\cosh r$ and $\sinh r$, the zeroth-order approximation $r_0 = 1.59$ to r is obtained. Rearranging the definition of r in Eq. (A.6) gives

$$\beta_d = r^2 - \frac{1}{4} U_d^2, \quad (\text{A.13a})$$

or, as a zeroth-order approximation,

$$\beta_d \cong \beta_{d0} = r_0^2 - \frac{1}{4} = 2.28 \quad (\text{A.13b})$$

using

$$\beta = \beta_d D / \mathcal{E}_I^2 = 2\beta_d \hbar \omega_{ph} \gamma_L \mathcal{E}^2 / \mathcal{E}_I^2 E_{V0}^2. \quad (\text{A.14a})$$

Thus Eq. (A.13b) yields

$$\beta_0 = 4.57 \hbar \omega_{ph} \gamma_L \mathcal{E}^2 / \mathcal{E}_I^2 E_{V0}^2. \quad (\text{A.14b})$$

By setting $\beta_0 = 51/t_p$, the breakdown field can be calculated from Eq. (A.14b):

$$E_{B0} = \left[\frac{1}{4.57} \frac{\mathcal{E}_I}{\mathcal{E}} \left(\frac{51 \mathcal{E}_I}{\hbar \omega_{ph} \gamma_L t_p} \right) E_{V0}^2 \right]^{1/2} = (0.219 \mathcal{E}_I / g \mathcal{E})^{1/2} E_{V0}. \quad (\text{A.15})$$

A better approximation is obtained by calculating the next-order term in β and E_B using a double Taylor expansion about U_d and r in Eq. (A.9):

$$2 \exp \left[-\frac{1}{2} (U_{d0} + \epsilon) \right] = \cosh (r_0 + \delta) - \frac{(U_{dn} + \epsilon)}{2(r_0 + \delta)} \sinh (r_0 + \delta). \quad (\text{A.16})$$

Expanding and equating first-order terms gives $\delta = -0.336\epsilon$ and

$$\beta_d = (r_0 + \delta)^2 - \frac{1}{4} = r_0^2 - \frac{1}{4} + 2r_0\delta + \frac{1}{2}\epsilon = \beta_{d0} + \beta_{d1} ,$$

$$\beta_{d1} = 2r_0\delta + \frac{1}{2}\epsilon = -0.570\epsilon . \quad (\text{A.17})$$

Since $U_d = (1 - E_d^2)/E_d^2 = -1 + 1/E_d^2 = U_{d0} + U_{d1}$, then

$$\beta_{d1} = -0.570/E_d^2 = -0.570E_{V0}^2/E^2 .$$

Thus, in the limit of $E^2 \gg E_{V0}^2$,

$$\beta \approx 4.57\hbar\omega_{\text{ph}}\gamma_L\mathcal{E}(E^2 - 0.57E_{V0}^2)/\mathcal{E}_I^2E_{V0}^2$$

and

$$E_B \approx (0.219\mathcal{E}_I/g\mathcal{E})^{1/2}E_{V0} .$$

Appendix B

AN ANALYTIC EXPRESSION FOR THE MULTIPLICATION RATE β
IN THE LIMIT OF A WEAK ELECTRIC FIELD

Here we derive an expression for the electron multiplication rate β appearing in Eq. (3.6), in the limit that the laser field E is weak. We begin by substituting Eq. (2.6) into Eq. (3.1) to find

$$\beta n(\mathcal{E}) + \partial J / \partial \mathcal{E} = 0 , \quad (\text{B.1})$$

which, upon integrating over energy from $\mathcal{E} = 0$ to $\mathcal{E} = \mathcal{E}_I$, yields the following general expression for β :

$$\beta = \frac{J(\mathcal{E}_I)}{\int_0^{\mathcal{E}_I} d\mathcal{E} n(\mathcal{E})} . \quad (\text{B.2})$$

We used the boundary condition in Eq. (3.5) to obtain this result.

Now in the limit of very small laser fields E , the electron multiplication rate β will also be very small--as demonstrated by physical considerations as well as the numerical calculations presented in Secs. III through V. For very small values of β , the term $\beta n(\mathcal{E})$ in Eq. (B.1) may be ignored everywhere, and--for all energies save those near the bottom of the band where electrons are injected--we have

$$\partial J / \partial \mathcal{E} = 0 , \quad (\text{B.3})$$

or

$$J(\mathcal{E}) = V(\mathcal{E})n(\mathcal{E}) - D(\mathcal{E}) \partial n / \partial \mathcal{E} = J(\mathcal{E}_I) , \quad (\text{B.4})$$

a relation that holds for all values of \mathcal{E} except those near zero.

Equation (B.4) is an elementary differential equation, and may be integrated at once, subject to the boundary condition $n(\mathcal{E}_I) = 0$. The result is

$$n(\mathcal{E}) = J(\mathcal{E}_I) \exp \left[\int_0^{\mathcal{E}} d\mathcal{E}'' \frac{V(\mathcal{E}'')}{D(\mathcal{E}'')} \right] \int_{\mathcal{E}}^{\mathcal{E}_I} \frac{d\mathcal{E}'}{D(\mathcal{E}')} \exp \left[- \int_0^{\mathcal{E}'} d\mathcal{E}'' \frac{V(\mathcal{E}'')}{D(\mathcal{E}'')} \right] . \quad (\text{B.5})$$

Hereafter we use Eq. (B.5) in combination with the low-field forms

$$V(\mathcal{E}) = - \hbar \omega_{ph} \gamma_L \quad (\text{B.6a})$$

and

$$D(\mathcal{E}) = \frac{2e^2 E^2}{3m^*} \frac{\mathcal{E} \gamma_k(\mathcal{E})}{\omega^2 + \gamma_k^2(\mathcal{E})} . \quad (\text{B.6b})$$

The central quantity is the integral

$$q(\mathcal{E}) = \int_0^{\mathcal{E}} d\mathcal{E}' V(\mathcal{E}') / D(\mathcal{E}') , \quad (\text{B.7})$$

which is a negative definite function of energy, with maximum absolute value at $\mathcal{E} = \mathcal{E}_I$. In fact, in very low fields, we have $|q(\mathcal{E}_I)| \gg 1$, and also $|\mathcal{E}_I q'(\mathcal{E}_I)| \gg 1$. The second integral in Eq. (B.5) is controlled by the contributions from energies very close to \mathcal{E}_I , so we have

$$\int_{\xi}^{\xi_I} \frac{d\xi'}{D(\xi')} \exp [-q(\xi')] \cong \frac{\exp [-q(\xi_I)]}{D(\xi_I)} \int_{\xi}^{\xi_I} d\xi' \exp [-(\xi' - \xi_I)q'(\xi_I)]$$

$$\cong \frac{\exp [-q(\xi_I)] - \exp [-q(\xi)]}{|V(\xi_I)|} . \quad (\text{B.8})$$

For $n(\xi)$, therefore, we have

$$n(\xi) = \frac{J(\xi_I)}{|V(\xi_I)|} \left\{ \exp [q(\xi) - q(\xi_I)] - 1 \right\} \quad (\text{B.9a})$$

$$\cong \frac{J(\xi_I)}{|V(\xi_I)|} \exp [q(\xi) - q(\xi_I)] , \quad (\text{B.9b})$$

where the factor of unity in Eq. (B.9a) is important only very close to $\xi = \xi_I$, a region that contributes little to the denominator in Eq. (B.2).

If we use the form for Eq. (B.9b) in Eq. (B.2), then we have

$$\beta = |V(\xi_I)| \frac{\exp [q(\xi_I)]}{\int_0^{\xi_I} d\xi \exp [q(\xi)]} , \quad (\text{B.10})$$

or, using explicit forms for the various quantities given above,

$$\beta = i\omega_{ph}\gamma_L(\omega_I) \frac{\exp \left\{ -\frac{3m^*}{e^2\epsilon_0^2} \int_0^{\omega_I} d\xi \frac{i\omega_{ph}\gamma_L(\xi)}{\xi\gamma_k(\xi)} [\omega^2 + \gamma_k^2(\xi)] \right\}}{\int_0^{\omega_I} d\xi \exp \left\{ -\frac{3m^*}{e^2\epsilon_0^2} \int_0^{\xi} d\xi' \frac{i\omega_{ph}\gamma_L(\xi')}{\xi'\gamma_k(\xi')} [\omega^2 + \gamma_k^2(\xi')] \right\}} .$$

(B.11)

REFERENCES

*Permanent addresses are as follows: D. L. Mills and A. A. Maradudin, University of California at Irvine, Irvine, California; T. Holstein, University of California at Los Angeles, Los Angeles, California; L. J. Sham, University of California at San Diego, La Jolla, California; and E. Loh, Jr., Malibu, California.

1. M. Van Marum, *Ann. Physik* 1, 68 (1799).
2. The following should lead the reader into the vast literature:
(a) J. J. O'Dwyer, The Theory of Electrical Conduction and Break-down in Solid Dielectrics (Clarendon, Oxford, 1973); (b) N. Bloembergen, *IEEE J. Quantum Electron.* QE-10, 375 (1974); (c) N. Klein, *Adv. Electron. and Electron. Phys.* 26, 309 (1969); (d) D. W. Fradin, Harvard University Technical Report 643, Contract N00014-67-A-0298-0006 (May 1973).
3. F. Seitz, *Phys. Rev.* 76, 1376 (1949).
4. W. Shockley, *Czech. J. Phys. B* 11, 81 (1961) and *Solid-State Electron.* 2, 35 (1961).
5. M. Bass and H. H. Barrett, *IEEE J. Quantum Electron.* QE-8, 338 (1971).
6. J. M. Ziman, Electrons and Phonons, edited by N. F. Mott, E. C. Bullard, and D. H. Wilkinson (Clarendon, Oxford, 1960).
7. K. K. Thornber and R. P. Feynman, *Phys. Rev. B* 1, 4099 (1970).
8. E. Yablonovitch, *Appl. Phys. Lett.* 19, 495 (1971).

9. D. W. Fradin, E. Yablonovitch, and M. Bass, *Appl. Opt.* 12, 700 (1973); D. W. Fradin, Harvard University Technical Report 643, Contract N00014-67-A-0298-0006 (May 1973).
10. W. L. Smith, J. H. Bechtel, and N. Bloembergen, *Phys. Rev. B* 15, 4039 (1977).
11. F. Seitz, *Phys. Rev.* 73, 549 (1948).
12. B. G. Gorshkov, Y. K. Danileiko, A. F. Epifanov, V. A. Lobachev, A. A. Manenkov, and A. V. Sidorin, *Sov. Phys.-JETP* 45, 612 (1977).
13. A. A. Manenkov, in Laser-Induced Damage in Optical Materials, edited by A. J. Glass and A. H. Guenther (National Bureau of Standards, Washington, D.C., Special Publication 509, 1977).
14. A. Schmid, P. Kelly, and P. Braeunlich, *Phys. Rev. B* 16, 4569 (1977).
15. R. Hellwarth, in Laser-Induced Damage in Optical Materials, edited by A. J. Glass and A. H. Guenther (National Bureau of Standards, Washington, D.C., Special Publication 341, 1970), p. 67.
16. L. H. Holway and D. W. Fradin, *J. Appl. Physics* 46, 279 (1975).
17. M. Sparks, "Theory of electron-avalanche breakdown in solids," in Laser-Induced Damage in Optical Materials, edited by A. J. Glass and A. H. Guenther (National Bureau of Standards, Washington, D.C., Special Publication 435, 1975), p. 331; M. Sparks, in Theoretical Studies of High-Power Ultraviolet and Infrared Materials (Xonics, Inc., Fifth Technical Report, Contract DAHE 15-73-C-0127, 30 June 1975), Secs. B and C.
18. M. Sparks, T. Holstein, R. Warren, D. L. Mills, A. A. Maradudin, L. J. Sham, E. Loh, Jr., F. King, in Laser-Induced Damage in

- Optical Materials, edited by A. J. Glass and A. H. Guenther (National Bureau of Standards, Washington, D.C., Special Publication 568, 1979), p. 467.
19. M. Sparks, R. Warren, T. Holstein, and D. L. Mills, 1980 (unpublished).
 20. T. Holstein, Phys. Rev. 70, 367 (1946); T. Holstein, in Theoretical Studies of High-Power Ultraviolet and Infrared Materials, Seventh Technical Report, 30 June 1976, ARPA Contract DAHC-15-73-C-0127.
 21. M. Sparks, "Electron-avalanche breakdown in solids--summary of results," June 1979 (unpublished).
 22. H. Fröhlich and N. F. Mott, Proc. R. Soc. London A 171, 496 (1939); H. Fröhlich, Proc. R. Soc. London A 160, 230 (1937); H. Fröhlich, Adv. Phys. 3, 325 (1954).
 23. J. M. Ziman, Principles of the Theory of Solids, 2nd ed. (Cambridge University, London, 1972).
 24. J. M. Ziman, Electrons and Phonons (Oxford University, London, 1960).
 25. D. W. Fradin, N. Bloembergen, and J. P. Letellier, Appl. Phys. Lett. 22, 635 (1973).
 26. M. J. Soileau, M. Bass, and E. W. Stryland, in Laser-Induced Damage in Optical Materials, edited by A. J. Glass and A. H. Guenther (National Bureau of Standards, Washington, D.C., Special Publication 541, 1978), p. 309.
 27. J. M. Aaron, C.L.M. Ireland, and C. Grey Morgan, J. Phys. D 7, 1907 (1974).

Table I. Influence on the breakdown threshold E_B of including various effects in the theory.

Including this effect in the theory causes the theoretical E_B to:	Increase	Decrease
Spherical aberrations	X	
Self-focusing		X
Macroscopic inclusions		X
Sample surface effects		X
Impurity levels in the bandgap		X
Control of E_B by starting electrons	X	
Electron or thermal diffusion out of the focal volume	X	
Raman scattering	X^a	X^b
Large quantum nature of $h\nu$		X
Multiphoton absorption		X
Inter-conduction-band transitions		X

NOTE: Experimentally measured extrinsic values are lower than the intrinsic theoretical values.

^aFor increasing focal diameter.

^bAs photon frequency increases.

Table II. Parameters used in numerical calculations.

Parameter	Definition	Value for NaCl of 293 K
$\hbar\omega_{ph}$	Phonon energy	(1/31) eV
ξ_I	Exciton threshold	7.8 eV
ϵ_∞	High-frequency dielectric constant	2.34
ϵ_0	Static dielectric constant	5.62
n_a	Atomic density	$2.24 \times 10^{-23} \text{ cm}^{-3}$
Q_a	Halide atomic cross section	0.35 nm^2
$M(\xi)$	Lattice mass	$\left\{ \begin{array}{l} 9.77 \times 10^{-23} \text{ g, } \xi < \frac{1}{2} \xi_{BZ} \\ 5.93 \times 10^{-23} \text{ g, } \xi > \frac{1}{2} \xi_{BZ} \end{array} \right.$
ξ_{BZ}	Electron energy at Brillouin zone edge	4.56 eV
$m^*(\xi)$	Electron effective mass	$\left\{ \begin{array}{l} \frac{1}{2} m, \xi \leq \frac{1}{2} \xi_{BZ} \\ m(\xi/\xi_{BZ}), \frac{1}{2} \xi_{BZ} \leq \xi \leq \xi_{BZ} \\ m, \xi \geq \xi_{BZ} \end{array} \right.$

FIGURE CAPTIONS

- Figure 1. Variation of the electron-momentum relaxation rate γ_k with energy (solid curve) for sodium chloride at room temperature. The individual contributions from Fröhlich scattering (longitudinal-optical) and from scattering by acoustical phonons are shown as dashed lines.
- Figure 2. Variation of the electron-energy loss rate γ_L with energy (solid curve) for sodium chloride at room temperature. The individual contributions from Fröhlich scattering (longitudinal-optical) and from scattering by acoustical phonons are shown as dashed lines.
- Figure 3. Variation of both the electron-momentum relaxation rate γ_k and the electron-energy loss rate γ_L with energy for sodium chloride at room temperature.
- Figure 4. Variation of the electron multiplication rate β with electric field for sodium chloride at several temperatures at $1.06 \mu\text{m}$.
- Figure 5. Variation of the electron multiplication rate β with electric field for sodium chloride at several temperatures at $10.6 \mu\text{m}$.
- Figure 6. Comparison of the experimental¹³ and theoretical values for the temperature dependence of E_B for sodium chloride at $1.06 \mu\text{m}$ and $10.6 \mu\text{m}$.
- Figure 7. Comparison of the experimental¹³ and theoretical values for the room-temperature breakdown field for several alkali halides at $1.06 \mu\text{m}$.

Figure 8. Comparison of the experimental¹³ and theoretical values for the room-temperature breakdown field for sodium chloride at 1.06 μm for various pulse durations.

Figure 9. Plot of E_{V0} , defined in Eq. (2.6), for sodium chloride at room temperature. Dotted lines indicate the values of the breakdown field E_B calculated from the rectangular barriers shown by dashed lines.

